Updating Potential Runaway Motion Volume in Task Space and Introducing Minimum Volume Enclosing Ellipsoid

Hiroki Kito, Yoji Yamada, Jian Liu, Shogo Okamoto
Graduate School of Engineering
Nagoya University
Nagoya, Japan
e-mail: kito.hiroki@d.mbox.nagoya-u.ac.jp

2021 International Conference on Computer, Control and Robotics (ICCCR) | 978-1-7281-9035-8/20/$31.00 ©2021 IEEE | DOI: 10.1109/ICCCR49711.2021.9349379

***Abstract*—Human-robot collaboration (HRC) has gained considerable interest among researchers, particularly in the manufacturing field. In such systems, new risks that have not previously been considered may now need to be assessed. One of these risks is that of a robot and worker colliding with one another. To avoid such collisions, a definition of the separation distance between a robot and a worker is needed. According to the ISO10218-1 standard, the safety of a worker needs to be maintained even in the case of a single safety system fault. Therefore, in defining the separation distance, a single fault needs to be considered, so that a robotic manipulator may safely run away when it occurs. As a method to quantify running away, a potential runaway motion in the task space (PRAM-t) was proposed. In the PRAM-t, a dynamic manipulability ellipsoid was used to calculate the acceleration as the robot runs away. However, when we consider running away originating from a single fault, it can be exaggerated. Therefore, this paper proposes a new method to compute acceleration during the running away of a robot using an algorithm to compute minimum volume enclosing ellipsoids. The proposed method and the dynamic manipulability ellipsoid (DME) method are compared using a case study.**

Keywords-human robot collaboration; dynamic manipulability; potential runaway motion in task space; single fault

I. INTRODUCTION

With the introduction of human-robot collaboration (HRC) which has been intensively discussed [1], hazardous impacts caused by collisions between industrial robots and workers are considered to be typical of the risks due to foreseeable misuse on the worker's side as well as to possible faults on the robot controller's side. According to the ISO10218-1 standard [2] [3], it is required that the safety of a worker is secured even in the case of a single fault within the safety related system, and that the same principle of single-fault detection and protective measures such as safety stops must be taken on the robot side. When risks in the output reliability block [3] are taken into account, it is necessary to define an environment where safety can be maintained in consideration of runaway due to a single fault of the robot. Protective separation distance (PSD), quantitatively indicating the minimum protection separation distance [2], is the target of safety requirements at manufacturing sites. The appendix of [5] shows the safety distance considering the relative motion vectors of both a robot and a human approaching it. in the case of personal care robots coexisting with humans as well.

Szabo et al. used a laser scanner-type of safety-related sensors in the SSM prototype for the first time [6]. The safety and productivity of the SSM functionality was evaluated by Marvel et al. [7] And they also conduct several curious research about PSD function [8]-[10].

On the other hand, Byner et al. maximized the efficiency of SSM by geometrically computing the distance of the robot to the source of danger [9]. Lacevic et al expands the SSM function to entire joints of the robot using a danger field algorithm for calculating avoidance motion [12], [13]. A number of studies have investigated the parameters that supplement the PSD, such as basic parameters [14] and the likelihood of intrusion [15]. Some researchers tried to introduce psychological parameters to PSD. If a human can avoid the robot itself, they do not collide. So avoidance actions were investigated from the view point of safety [16]-[18].

Let us consider a relationship between a safety of HRC and a single fault. A fault detection algorithm also being researched actively. Brambilla et al. proposed fault detection for robot manipulators via second-order sliding modes [19]. And same one via high-order sliding mode also be investigated [20]. And a robust fault diagnosis and fault-tolerant control system using high-order sliding mode is presented [21].

This time, we will define the runaway action of a manipulator. The runaway action assumed in this study is attributed to a single fault of the output robot. In addition, the most hazardous events shall be assumed when discussing safety. Considering these two points, it can be said that the event that we must assume is that of the robot joint causing a single fault and the joint torque being maximized. Furthermore, because industrial robots have a self-diagnosis function, if a single fault such as one described above occurs, the robot itself will detect it, and apply a brake after a certain reaction time.

In summary, phases in a PSD process in association with the robot runaway is decomposed as follows:

1. The output torque of one of the robot's joints is maximized due to a single fault.
2. After a reaction time, the joint is braked, decelerating the robot.
3. The robot is stopped completely.

In this paper, the above three steps are defined as "runaway." Yamada et al. defined the space in which a robot can move before an emergency stop during a runaway as a potential runaway space in the task space expression (PRAM-t), and calculated the runaway distance using the concept of a dynamic manipulability ellipsoid (DME) [24].

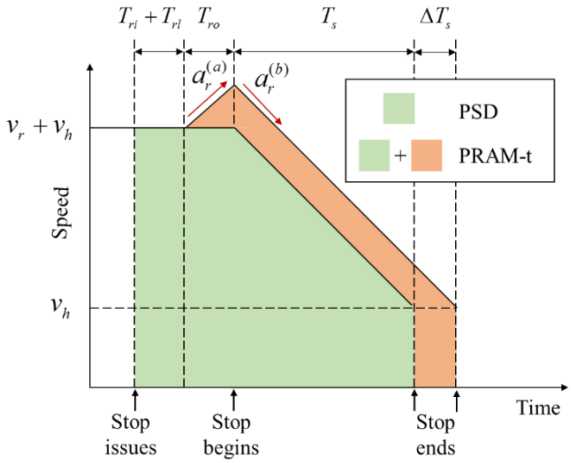

Figure 1." An illustration of PSD and PRAM-t.

Figure 1 illustrates a sample speed pattern which includes both PSD (green colored area) and PRAM-t (orange-colored area), where v_h and v_r denote the relative speed of the operator and the robot, respectively, and which define the closest distance plane; T_{ri}, T_{rl}, and T_{ro} denote the reaction time of the protective equipment, logical control device, and motor drive respectively. T_s, and ΔT_s represent the stopping time to make the speed of the robot zero and an increase in the stopping time due to the acceleration of the robot system respectively. Finally, $a_t^{(a)}$ and $a_r^{(b)}$ denote acceleration and deceleration performance of the robot, respectively.

In the PRAM-t, the DME is introduced as a method for computing acceleration when a robot runs away due to a single fault. However, when we reconsider it, the constraint of a DME is appropriate under our assumption. In other words, we should make the DME constraints stricter. Therefore, we propose introducing an algorithm for the computation of minimum volume enclosing ellipsoids (MVCE) to the DME. In this paper, we refer to it as a DME under the assumption of a single fault (DMESF) and suggest to update PRAM-t by introducing DMESF as an alternative of DME. And we also rename updated PRAM-t, as a potential runaway motion in task space under the assumption of a single fault, (PRAM-sf). Then we compare the DME and the DMESF using a case study as a pre-step of proposing PRAM-sf.

II. Potential Runaway Motion in the Task Space

A. *Dynamic Manipulability Ellipsoid*

Yoshikawa et al. proposed the concept of manipulability measure of robotic mechanisms, as discussed in [23]. This is a measure of the manipulating ability of robotic mechanisms in positioning and orienting end-effectors. They also proposed a dynamic manipulability measure of robot arms as a quantitative measure of their manipulating ability in positioning and orienting the end-effectors, which takes the arm dynamics into consideration [24]. Furthermore, new DMEs were proposed. Chiacchio et al. [26] researched the influence of gravity on the manipulators. In addition, for redundant manipulators [27], the velocity-dependent dynamic manipulability [28] was researched. And as an extended concept of dynamic manipulability, the dynamic property of multi fingered grasping systems consisting of a multi fingered hand and a grasped object was evaluated [29].

Since this concept is used in the PRAM-t, we start from a brief introduction of the theory. When there are no disturbances, the equation of motion for an open-chain manipulator with n rigid links can be expressed as:

$$\boldsymbol{\tau} = \boldsymbol{M}(\boldsymbol{q})\ddot{\boldsymbol{q}} + \boldsymbol{\tau}_c(\boldsymbol{q},\dot{\boldsymbol{q}}) + \boldsymbol{\tau}_g(\boldsymbol{q}) \tag{1}$$

where $\boldsymbol{\tau}$ is an $n \times 1$ vector of joint actuator torques and $\boldsymbol{q}$, $\dot{\boldsymbol{q}}$ and $\ddot{\boldsymbol{q}}$ are $n \times 1$ vectors of joint angles, joint angular velocities, and joint angular accelerations, respectively. $\boldsymbol{M}(\boldsymbol{q})$ is the $n \times n$ mass matrix that comes from the inertial properties of the robot, $\boldsymbol{\tau}_c(\boldsymbol{q},\dot{\boldsymbol{q}})$ represents the vector of Coriolis and centrifugal forces, and $\boldsymbol{\tau}_g(\boldsymbol{q})$ represents the vector of joint torque that comes from gravity. Let us define the vector of the position of the tip of the robot as $\boldsymbol{x}$ ($m \times 1$). In this study, we only consider translational acceleration. Thus, we can say that $m \leq 3$. Using the $m \times n$ Jacobian matrix $\boldsymbol{J}$, we can obtain the relationship between $\dot{\boldsymbol{x}}$ and $\dot{\boldsymbol{q}}$.

$$\dot{\boldsymbol{x}} = \boldsymbol{J}(\boldsymbol{q})\dot{\boldsymbol{q}} \tag{2}$$

This equation can also be obtained by differentiating (2) with respect to time.

$$\ddot{\boldsymbol{x}} = \boldsymbol{J}(\boldsymbol{q})\ddot{\boldsymbol{q}} + \dot{\boldsymbol{J}}(\boldsymbol{q},\dot{\boldsymbol{q}})\dot{\boldsymbol{q}} \tag{3}$$

The mass matrix $\boldsymbol{M}$ is positively defined and invertible. Therefore, using Eq. (1) and Eq. (3), we can obtain the following equations:

$$\ddot{\boldsymbol{x}} = \boldsymbol{J}\boldsymbol{M}^{-1}(\boldsymbol{\tau} - \boldsymbol{\tau}_c - \boldsymbol{\tau}_g) + \dot{\boldsymbol{J}}\dot{\boldsymbol{q}} \tag{4}$$

$$\ddot{\boldsymbol{x}} = \boldsymbol{J}\boldsymbol{M}^{-1}\boldsymbol{\tau} + \ddot{\boldsymbol{x}}_{vel} + \ddot{\boldsymbol{x}}_{grav} \tag{5}$$

where:

$$\ddot{\boldsymbol{x}}_{vel} = -\boldsymbol{J}\boldsymbol{M}^{-1}\boldsymbol{\tau}_c + \dot{\boldsymbol{J}}\dot{\boldsymbol{q}} \tag{6}$$

$$\ddot{\boldsymbol{x}}_{grav} = -\boldsymbol{J}\boldsymbol{M}^{-1}\boldsymbol{\tau}_g \tag{7}$$

It is imperative to consider torque limits as well.

$$-\tau_i^{\max} \leq \tau_i \leq \tau_i^{\max}, \qquad i = 1,\cdots,n \tag{8}$$

If the torque limits are symmetric, as in (8), $\hat{\boldsymbol{\tau}}$ which is the normalized $\boldsymbol{\tau}$ is given by:

$$\hat{\boldsymbol{\tau}} = [\tau_1 / \tau_1^{\max}, \cdots, \tau_n / \tau_n^{\max}] \tag{9}$$

Here, let us introduce $\boldsymbol{L}$ where,

$$\boldsymbol{L} = diag(\tau_1^{\max}, \cdots, \tau_n^{\max}) \tag{10}$$

$$\hat{\boldsymbol{M}} = \boldsymbol{M}^{-1}\boldsymbol{L} \tag{11}$$

Using Eq. (11) with Eq. (5), we obtain Eq. (12) as

$$\ddot{\boldsymbol{x}} = \boldsymbol{J}\hat{\boldsymbol{M}}\hat{\boldsymbol{\tau}} + \ddot{\boldsymbol{x}}_{vel} + \ddot{\boldsymbol{x}}_{grav} \tag{12}$$

We can interpret $\ddot{\boldsymbol{x}}_{vel} + \ddot{\boldsymbol{x}}_{grav}$ as a bias of the end-effector acceleration with no torque. When we focus on the term $\boldsymbol{J}\hat{\boldsymbol{M}}\hat{\boldsymbol{\tau}}$, $\boldsymbol{J}\hat{\boldsymbol{M}}\hat{\boldsymbol{\tau}}$ is represented as an ellipsoid because $\|\hat{\tau}_i\| \leq 1$. If the singular value decomposition is $\boldsymbol{J}\hat{\boldsymbol{M}}$ as in Eqs. (13)-(16), the spindles can be obtained as $\sigma_1\boldsymbol{u}_1, \cdots, \sigma_m\boldsymbol{u}_m$.

$$\boldsymbol{J}\hat{\boldsymbol{M}} = \boldsymbol{U}\boldsymbol{\Sigma}\boldsymbol{V}^{\mathrm{T}} \tag{13}$$

$$\boldsymbol{U} = \left[\boldsymbol{u}_1, \cdots, \boldsymbol{u}_m\right] \tag{14}$$

$$\boldsymbol{\Sigma} = \left[\begin{array}{ccc|c} \sigma_1 & & 0 & \\ & \ddots & & 0 \\ 0 & & \sigma_m & \end{array}\right] \tag{15}$$

$$\boldsymbol{V} = \left[\boldsymbol{v}_1, \cdots, \boldsymbol{v}_n\right] \tag{16}$$

(Note that $\boldsymbol{U}, \boldsymbol{\Sigma}, \boldsymbol{V}$ is $m \times m$, $m \times n$, and $n \times n$, respectively). Spindles of the DME can be obtained as $\sigma_1\boldsymbol{u}_1, \cdots, \sigma_m\boldsymbol{u}_m$.

B. Otential Runaway Motion in the Task Space

If the manipulator breaks down and runs away, it is possible that the manipulator will take a different trajectory from its normal trajectory. Since this research is aimed at the collaborative operation of industrial manipulators in a manufacturing environment, it can be assumed that the manipulator has a self-diagnosis function. In other words, it is possible to terminate the manipulator in a stopped state after a certain time (reaction time) from the state at which the fault is detected by itself and causes the manipulator to run away.

When the manipulator breaks down and begins to run away, the speed each joint will output is uncertain. Under this condition, the manipulator's end effector moves during the time to reach the stop state and it will be positioned indeterminately within a certain range. This is called the potential runaway motion in the task space (PRAM-t) [22].

In PRAM-t, it is necessary to check the upper limit maximum velocity of the manipulator in advance and determine whether the velocity of the manipulator reaches this upper limit velocity during the reaction time. The manipulator velocity pattern when the it reaches the upper limit maximum velocity due to acceleration during runaway is determined as Speed Pattern 1, and in the same case, the manipulator velocity pattern when it does not reach the upper limit maximum velocity is determined as Speed Pattern 2. These are shown in Figure 1, the left side depicting the former and the right side depicting the latter.

In both graphs, the horizontal axis represents time, and the vertical axis represents the velocity of the manipulator. v_R is the velocity of the manipulator when a single fault occurs, $v_{\max}$ is the upper limit maximum velocity of the manipulator, t_R is the reaction time, and the area of each graph shows the runaway distance.

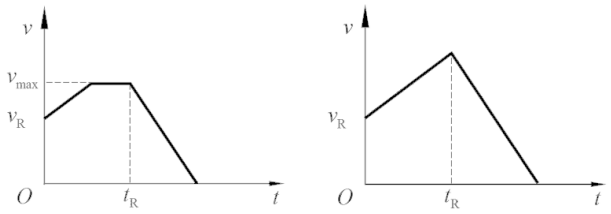

Figure 2." Relationship between manipulator velocity and time.

III. Dynamic Manipulability Ellipsoid under the Assumption of a Single Fault

A. Disadvantage of the Original PRAM-t

The potential runaway motion in a task space is a useful technique for visually expressing the manipulator's behavior during runaway.

However, in some cases, the space obtained using this method may overestimate the space where the manipulator can run away. When we calculate the potential runaway space of the workspace representation, a driving force may be generated at multiple joints. Because we consider a single fault, it is impossible for multiple joints to generate a driving force. Therefore, the latent runaway space in the workspace expression includes a space that cannot be reached in the event of a single fault. Defining a space larger than necessary should be less productive because it leads to low work efficiency and requires a larger task space at the manufacturing site. In the subsequent sections, we propose a method to calculate the net latent runaway space at the time of a single fault and explain the concept and algorithm of the minimum volume enclosing ellipsoid used in the method. As we wrote in introduction, we suggest to update PRAM-t by introducing DMESF as an alternative of DME. And we also rename updated PRAM-t, as a potential runaway motion in task space under the assumption of a single fault, (PRAM-sf).

B. Minimum Volume Enclosing Ellipsoid

In this section, we discuss the algorithm for the minimum volume enclosing ellipsoid (MVCE). In [30], the authors proposed a method for rounding polytopes in the real number model of computation, after which it was updated by [33]. In [31], a minimum enclosing polytope in high dimensions was proposed. In [32], the computation of the MVCE was researched.

It would be useful to explain its properties briefly. Consider a set of m points in an n-dimensional space, $\boldsymbol{S} = \{\boldsymbol{x}_1, \cdots, \boldsymbol{x}_m\} \subset \mathbf{R}^n$. To guarantee that any ellipsoid containing $\boldsymbol{S}$ has a positive volume, we assume that the affine hull of the $\boldsymbol{S}$ spans $\mathbf{R}^n$. An ellipsoid in center form is given by:

$$\varepsilon = \{x \in \mathbf{R}^n \,|\, (x-c)^{\mathrm{T}} E (x-c) \le 1\} \tag{17}$$

where $c \in \mathbf{R}^n$ denotes the center of the ellipsoid ε and $E \in S^n_{++}$.

Since we want points x_i to be inside ε, they must satisfy

$$(x-c)^{\mathrm{T}} E (x-c) \le 1 \qquad i = 1, \cdots, m. \tag{18}$$

The volume of ε is given by:

$$\mathrm{Vol}(\varepsilon) = \frac{v_0}{\sqrt{\det(E)}} \tag{19}$$

where v_0 is the volume of the unit hypersphere in n-dimensional space. Considering these, a natural formulation of the minimum volume enclosing ellipsoid (MVEE) problem is described as follows:

$$\begin{aligned} &\text{minimize}_{E,c} \quad \det(E^{-1}) \\ &\text{subject to} \quad (x-c)^{\mathrm{T}} E (x-c) \le 1 \qquad i = 1, \cdots, m \\ &\qquad\qquad E > 0 \end{aligned} \tag{20}$$

However, Eq. (20) is not a convex optimization problem and, by a change of variable, we can define the ellipsoid as:

$$\varepsilon = \{x \in \mathbf{R}^n \,|\, \|Ax - b\|_2 \le 1\} \tag{21}$$

where $A = E^{1/2}$ and $b = E^{1/2} c$. Therefore, considering Eq. (21), the optimization problem (20) becomes:

$$\begin{aligned} &\text{minimize}_{A,b} \quad \log\det(A^{-1}) \\ &\text{subject to} \quad \|Ax_i - b\| \le 1 \qquad i = 1, \cdots, m \\ &\qquad\qquad A > 0 \end{aligned} \tag{22}$$

The norm constraints $\|Ax_i - b\| \le 1$, which are just convex quadratic inequalities in the variables A and b, can be expressed as follows:

$$\begin{bmatrix} I & Ax_i - b \\ (Ax_i - b)^{\mathrm{T}} & I \end{bmatrix} \ge 0 \tag{23}$$

In short, the optimization problem of the MVEE can be solved by changing variables A and b.

C. Dynamic Manipulability Ellipsoid under a Single Fault Assumption

In this section, we consider the method to calculate dynamic manipulability ellipsoid (DMESF). In order to calculate the DMESF, the following constraints are added to the joint torque vector. The constraint is that when the norm of normalized torque vector is less than 1 and the torque of the joint i is not 0 and others are 0. For example, the torque vector when a single fault occurs on the joint i is like this:

$$\begin{aligned} &\hat{\tau}_i = [0, \ldots, \hat{\tau}_i, \ldots, 0] \\ &\text{subject to} \quad |\hat{\tau}_i| \le 1 \end{aligned} \tag{24}$$

And using (15) and (24), the acceleration due to a single fault of the i joint $\ddot{x}_i$ can be obtain like this:

$$\ddot{x}_i = J\hat{M}\hat{\tau}_i + \ddot{x}_{vel} + \ddot{x}_{grav} \tag{25}$$

And then, we only need the largest acceleration due to a single fault of each joint in order to calculate DMESF using MVEE algorithm. We can obtain the set of largest accelerations due to a single fault of each joint like this:

$$\begin{aligned} &\hat{\tau}_{\pm i} = [0, \ldots, \pm 1, \ldots, 0] \\ &\ddot{x}_{\pm i} = J\hat{M}\hat{\tau}_{\pm i} + \ddot{x}_{vel} + \ddot{x}_{grav} \qquad i = 1, \ldots, n \end{aligned} \tag{26}$$

Finally, we can obtain DMESF by computing MVEE which including all $\ddot{x}_{\pm i}$.

IV. Comparison of DME and DMESF

A. Condition of Comparison

To investigate the usefulness of the proposed DMESF, we calculated the DME and the DMESF under the same conditions and compared their volumes. This time, we note the conditions of calculation. We chose KUKA's LBR iiwa 700 (KUKA) as the target manipulator for the comparison, as shown in Figure 3. where, Σ_B is the basic KUKA coordinate. We defined typical five configurations of KUKA, as shown in Figure 4 for the purpose of quantitatively evaluating the performance of proposed DMESF. In Figure 4, Σ_B is also the basic coordinate of KUKA.

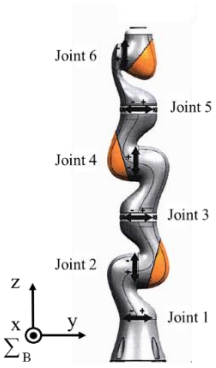

Figure 3." KUKA LBR iiwa 700.

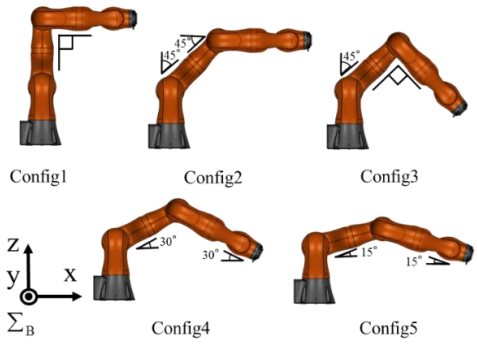

Figure 4." Different configurations defined for comparison.

B. *Results of Comparison*

Figures 5–9 show the DME and DMESF comparisons for each configuration. The axes of each graph show the directions of acceleration, and the coordinates for each graph are the same for the basic coordinate of KUKA. The circles depict the acceleration, $\ddot{\boldsymbol{x}}_{i+}, \ddot{\boldsymbol{x}}_{i-}(i=1,..,n)$, and the broken lines denote the DME and DMESF in their respective graphs. From these results, it can be seen that the DMESF is enveloped by the DME in all configurations.

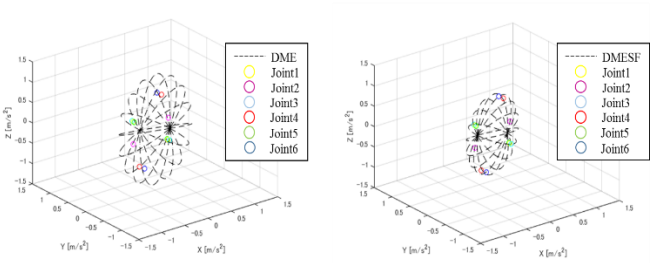

Figure 5." DME and DMESF for configuration 1.

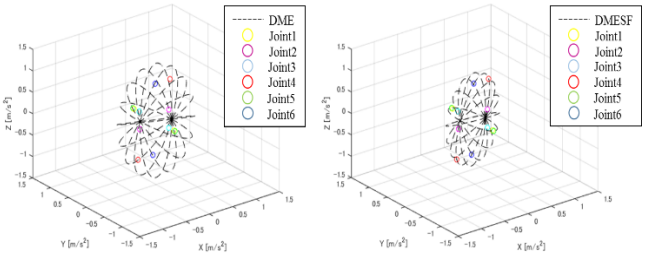

Figure 6." DME and DMESF for configuration 2.

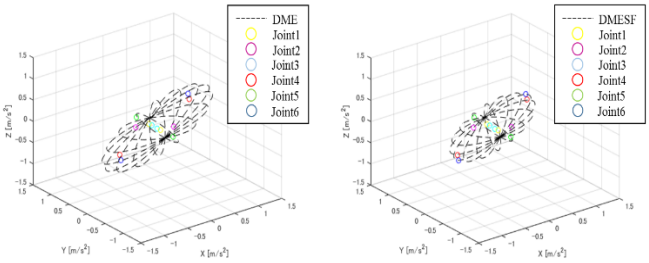

Figure 7." DME and DMESF for configuration 3.

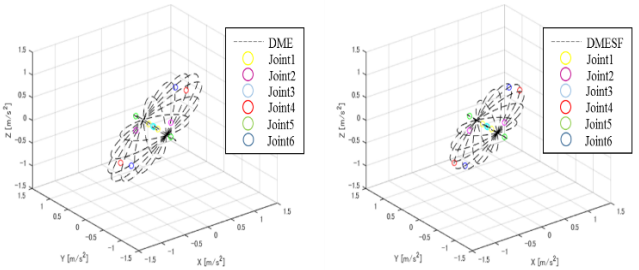

Figure 8." DME and DMESF for configuration 4.

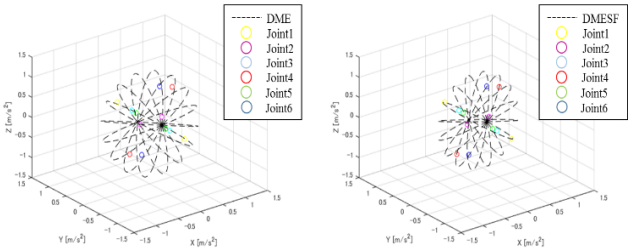

Figure 9." DME and DMESF for configuration 5.

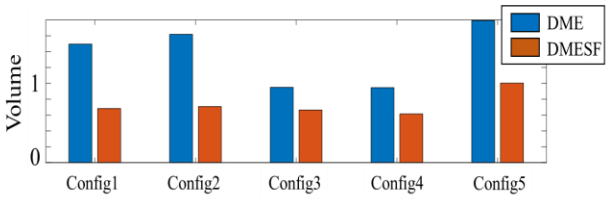

Figure 10."Comparison of volumes.

A comparison of the volumes is shown in Figure 9. The vertical axis shows the volume of the ellipsoid and the horizontal axis shows the configurations. The blue bar represents the DME and the orange bar represents the DMESF. From this result, it can be gauged that the volume of the DMESF is smaller than that of the DME under all conditions. If we use the DMESF instead of the DME, the calculated space becomes smaller, the reduction of which is important when we consider introducing the PRAMSF as the separation distance between a human and manipulator.

V. Discussion

In this work, we defined the worst case scenario due to a single fault on the output manipulator. It was that a torque of one joint becomes maximize. And we considered a computing algorithm of the DMESF under this scenario. However, strictly speaking, there is a more dangerous case example than the worst case we defined. The case is that multiple torques are generated and it can occur due to a common cause failure. Although multiple torques can be generated, the possibility of common cause failure is low enough not to be taken into account. Therefore we can ignore the scenario considering the concept of risk assessment.

The comparison (Figure 9) shows that the volume of DMESF is smaller than that of DME in all configurations. And the difference of volume vary greatly according to configurations. About configuration 2 and 3, the difference is relatively small and the benefit of introducing DMESF become small in such configuration.

Finally, there is room for the improvement of human robot collaboration tasks. The relationship between the worker's safety and the work space which depends on the separation distance is a tradeoff. The computation time of the method we proposed should be short enough to implement it in an on-line system. So, it is necessary to grasp the target problem as a multiple objective optimization one considering the worker's safety as the high priority.

VI. Conclusion

In this study, the PRAM-t was proposed as a method to represent the space in which a manipulator can move. In the potential runaway motion volume in the task space, a DME was used to compute the acceleration of the manipulator when a single fault occurred at joint *i* of the manipulator. Further, an alternative to the DME was proposed. We named it as DMESF; it is a method that combines dynamic manipulability and the algorithm for computing the MVEE. To evaluate the proposed method, we compared the DME and DMESF under the same conditions for different manipulator configurations. As a result, it was found that the DMESF is enveloped by the DME, and the volume of the DMESF is smaller than that of the DME. These results indicate that DMESF can represent the substantive torques which are generated due to a single fault. Therefore introducing the DMESF as an alternative to the DME is useful and achieves a reduction in space.

The approach to combining the dynamic manipulability and the method for computing a minimum volume enclosing ellipsoid can realize a reduction of a separation distance between a human and a manipulator while ensuring safety. This concept should contribute to the enhancement of safety in HRC tasks if it is visualized (e.g. on a simulator). Ongoing work following this research includes validating DMESF, computing PRAMSF, implementing PRAMSF to an on-line safety related system, and evaluating the performance of the PRAMSF as an alternative to the PRAM-t.

Acknowledgment

The authors would like to thank their colleague Kim Eugene for the provision of referential data.

References

[1] Kim, Eugene, et al. "Considerations of potential runaway motion and physical interaction for speed and separation monitoring." Robotics and Computer-Integrated Manufacturing 67: 102034.

[2] ISO 10218–1,Robots for individual requirements –Safety requirements, 2010

[3] Robots and robotic devices–Safety requirements for industrial robots–Part 2: Robot systems and integration, ISO 10218-2: 2011.

[4] ISO/TS 15066, Robots and robotic devices – Collaborative robots, 2016

[5] ISO 13482, Robots and robotic devices – Safety requirements for personal care robots, 2014.

[6] S. Szabo, W. Shackleford, R. Norcross, J. Marvel, A Testbed for Evaluation of Speed and Separation Monitoring in a Human Robot Collaborative Environment, US Department of Commerce, National Institute of Standards 565 and Technology, 2012

[7] J. A. Marvel, Performance metrics of speed and separation monitoring in shared workspaces, IEEE Transactions on Automation Science and Engineering 10 (2) (2013) 405–414.

[8] J. A. Marvel, R. Bostelman, A cross-domain survey of metrics for mod570 elling and evaluating collisions, International Journal of Advanced Robotic Systems 11 (9) (2014) 142. 33

[9] J. A. Marvel, J. Falco, I. Marstio, Characterizing task-based human–robot collaboration safety in manufacturing, IEEE Transactions on Systems, Man, and Cybernetics: Systems 45 (2) (2014) 260–275. 575

[10] J. A. Marvel, R. Norcross, Implementing speed and separation monitoring in collaborative robot workcells, Robotics and computer-integrated manufacturing 44 (2017) 144–155.

[11] C. Byner, B. Matthias, H. Ding, Dynamic speed and separation monitoring 585 for collaborative robot applications–concepts and performance, Robotics and Computer-Integrated Manufacturing 58 (2019) 239–252.

[12] B. Lacevic, P. Rocco, Kinetostatic danger field-a novel safety assessment for human-robot interaction, in: Intelligent Robots and Systems , 2010 580 IEEE/RSJ International Conference on, IEEE, 2010, pp. 2169–2174.

[13] B. Lacevic, P. Rocco, A. M. Zanchettin, Safety assessment and control of robotic manipulators using danger field, IEEE Transactions on Robotics 29 (5) (2013) 1257–1270

[14] D. Kuli´c, E. Croft, Pre-collision safety strategies for human-robot interaction, Autonomous Robots 22 (2) (2007) 149–164.

[15] A. R. Sanderud, M. Niitsuma, T. Thomessen, A likelihood analysis for a risk analysis for safe human robot collaboration, in: Emerging Technologies & 595 Factory Automation (ETFA), 2015 IEEE 20th Conference on, IEEE, 2015, pp. 1–6.

[16] K. SUNADA, Y. YAMADA, T. HATTORI, S. OKAMOTO and S. HARA, Extrapolation Simulation for Estimating Human Avoidability in Human-Robot Coexistence Systems, Proc. of IEEE International Symposium on Robot and Human Interactive Communication, Paris, pp. 785–790, 2012

[17] T. HATTORI, Y. YAMADA, S. MORI, S. OKAMOTO, and S. HARA, Psychological Experiments on Avoidance Action Characteristics for Estimating Avoidability of Harm to Eyes from Robots, Proc. of IEEE/RSJ International Conference on Intelligent Robots and Systems, pp, 5400–5405, 2012

[18] T. NISHIYAMA, Y. YAMADA, S. OKAMOTO, S. HARA, S. TAKEDA, Human Avoidance Action Characteristics against Approaching Motions of a Robot End Effector at Close Range Triggered by Human Errors, Proc. of TOKAI ENGINEERING COMPLEX 2015(TEC15), pp. 153–156, 2016 (in Japanese)

[19] D. Brambilla, L. M. Capisani, A. Ferrara, and P. Pisu, "Fault detection for robot manipulators via second-order sliding modes," IEEE Trans. Ind. Electron., vol. 55, no. 11, pp. 3954–3963, Nov. 2008

[20] L. M. Capisani, A. Ferrara, A. Ferreira De Loza, and L. M. Fridman, "Manipulator fault diagnosis via higher order sliding-mode observers," IEEE Transactions on Industrial Electronics, vol. 59, no. 10, pp. 3979–3986, 2012.

[21] Van, Mien, Pasquale Franciosa, and Dariusz Ceglarek. "Fault diagnosis and fault-tolerant control of uncertain robot manipulators using high-order sliding mode." Mathematical Problems in Engineering 2016.

[22] Y. Yamada, S. Takeda, T. Nishiyama and S. Okamoto: "Potential Runaway Motion Volume in Task Space for Estimating The Probability of Occurrence of A Human-Robot Collision," IEEE International Conference on Intelligence and Safety for Robotics, pp.34-39, 2018

[23] T. Yoshikawa, "Manipulability of robot mechanisms," Int. J. Robot. Res., vol. 4, no. 2, pp. 3–9, 1985

[24] T. Yoshikawa, "Dynamic manipulability of robot manipulators," J. Robot. Syst., vol. 2, no. 1, pp. 113–124, 1985

[25] R. Koeppe and T. Yoshikawa, "Dynamic manipulability analysis of compliant motion," in Proc. IEEE/RSJ Int. Conf. Intell. Robots Syst., 1997, pp. 1472–1478

[26] P. Chiacchio, S. Chiaverini, L. Sciavicco and B. Siciliano, "Influence of gravity on the manipulability ellipsoid for robot arms," ASME Journal of Dynamic Systems, Measurement and Control 114 723–727. (1992)

[27] P. Chiacchio, "New dynamic manipulability ellipsoid for redundant manipulators," Robotica, vol. 18, no. 4, pp. 381–387, 2000

[28] M. T. Rosenstein and R. A. Grupen, "Velocity-dependent dynamic manipulability," in Proc. IEEE Int. Conf. Robot. Autom., 2002, pp. 2424–2429

[29] Yokokohji, Yasuyoshi, Jose San Martin, and Masaki Fujiwara. "Dynamic manipulability of multifingered grasping." IEEE Transactions on Robotics 25.4 (2009): 947-954.

[30]" L. G. Khachiyan, Rounding of polytopes in the real number model of computation, Mathematics of Operations Research 21 (1996), 307–320

[31]" P. Sun and R. Freund, "Computation of minimum-volume enclosing ellipsoids," Oper. Res., vol. 52, no. 5, pp. 690–706, 2004

[32]" Kumar, P., Yildirim, E.: Minimum-volume enclosing ellipsoids and core sets. Journal of Optimization Theory and Applications 126, 1–21 (2005)

[33]" M. J. Todd and E. A. Yıldırım, On Khachiyan's algorithm for the computation of minimum volume enclosing ellipsoids, Discrete Appl. Math., 155 (2007), pp. 1731–1744